

RECENT RESULTS FROM SUPER-KAMIOKANDE

R. J. WILKES

Department of Physics, University of Washington, Seattle, WA 98195 USA

E-mail: wilkes@uw.edu

For

THE SUPER-KAMIOKANDE COLLABORATION^a

ABSTRACT

Selected recent results from Super-Kamiokande are reviewed, including searches for WIMPS and supernova relic neutrinos, solar neutrino updates, and tests of non-standard interaction models.

1. Introduction

Super-Kamiokande (SK), a 50 kton water Cherenkov detector, located under 2700 meters minimum water-equivalent rock overburden at the Kamioka Observatory in western Japan, has been taking data since 1996. SK has a cylindrical design, and is divided into two optically separated sections by a structural framework that supports the photomultiplier tubes (PMTs). During the SK-I running period, roughly 1996 to 2001, the inner detector (ID) was equipped with 11146 50cm PMTs aimed inward, and the outer detector (OD) volume had 1885 20cm PMTs, aimed outward and equipped with wavelength-shifting plastic plates. The OD functions primarily as a veto counter, tagging charged particles that enter or exit the ID. The SK-II running period (2002-2005) had approximately half as many active PMTs, due to the accidental implosion of many tubes in the ID and OD in 2001. For the SK-III running period (2006-2008), the full complement of PMTs was restored, with original front-end electronics. The SK-IV running period (2008-) has the same PMT configuration as SK-III, but with completely updated, deadtime-free data acquisition electronics.

Within the ID, a central 22.5 kiloton fiducial volume (FV) is defined, within which detector response is expected to be uniform. Fully-contained (FC) neutrino events are those where interaction products are observed in the ID, with no significant correlated activity in the OD, while partially-contained (PC) events are those where some interaction products exit the ID. Upward-going muons (upmus) are events where a penetrating particle traveling in the upward direction enters and either stops or passes through the detector, and are attributed to muons produced by neutrino interactions in the surrounding rock. In general terms, FC, PC, and upward muon events represent successively higher energy samples of neutrino interactions, ranging from 200 MeV for the lowest energy FC events to above 1 TeV for the highest energy upward-going

^aA complete list of current members of the Super-Kamiokande Collaboration can be found in Reference ¹⁶.

muons. Further details regarding the SK detector design, operation, calibrations, and data reduction can be found elsewhere ^{1) 2) 3)}.

2. WIMP Search

In minimal supersymmetric (MSSM) extensions of the Standard Model, the most well-motivated candidate for WIMPs is the neutralino ($\tilde{\chi}$) ⁴⁾. Given constraints from accelerator experiments and astrophysics, the neutralino mass is expected to be in the range from several tens of GeV to 10 TeV, depending on the models chosen ⁵⁾ ⁶⁾. SK is better suited than, for example, IceCube to search for WIMPs with mass below 100 GeV, due to its lower energy threshold for neutrino signals. Relative to previously reported WIMP search results from SK ⁷⁾, we have nearly doubled the size of the dataset of upmu, the category of neutrino events in SK with the highest mean energy, to 3109.6 live-days. In addition, the new analysis takes into account the neutrino energy dependence of detector response in order to improve the limit on the WIMP-induced upmu flux and SD cross section, and uses WIMPsim ⁸⁾ and the DARKSUSY simulator⁹⁾, to more accurately simulate the WIMP-induced neutrino fluxes and propagation. Details of the WIMP search analysis are provided in ¹⁰⁾.

The main background is upmu events due to atmospheric neutrinos. These were estimated using the NEUT neutrino interaction simulation package¹¹⁾, and a GEANT-based detector simulator, with input fluxes as calculated by Honda *et al.* ¹²⁾ and Volkova *et al.* ¹³⁾. In this analysis, the uncertainty in absolute neutrino flux is irrelevant, since we normalize by the number of upmu events in each category. Neutrino oscillations are taken into account, taking $\Delta m_{23}^2 = 0.0025\text{eV}^2$ and $\sin^2(2\theta_{23}) = 1.0$ from previous SK results ^{3) 14)}. We compared upward-going muon events with the estimated background of atmospheric neutrinos to search for a WIMP-induced neutrino signal from the direction of the Sun. No significant excess was observed. To calculate the upmu flux limits, we derived cone half-angles which would contain more than 90% of the upmu signal for each WIMP mass from the simulations, obtaining upmu flux limits as a function of WIMP mass for annihilation into $\bar{b} - b$ (soft) and W^+W^- (hard) annihilation channels.

The 90% C.L. upper limits of upward-going muon flux induced by WIMPs of $100\text{GeV}/c^2$ were $6.4 \times 10^{-15}\text{cm}^{-2}\text{sec}^{-1}$, and $4.0 \times 10^{-15}\text{cm}^{-2}\text{sec}^{-1}$ for the soft (Fig. 1) and hard (Fig. 2) annihilation channels, respectively. Our limit excludes part of the region of expected upmu flux estimated by some SUSY models. An upper limit on the spin-dependent scattering cross section was also obtained, using a WIMP mass-dependent conversion factor ¹⁵⁾. These (Fig. 3) correspond to upper limits of $4.5 \times 10^{-39}\text{cm}^{-2}$ and $2 \times 10^{-40}\text{cm}^{-2}$ for the soft and hard annihilation channels, respectively. At low WIMP mass (below 100 GeV) our limit on the WIMP-proton spin-dependent cross section is better than current results from both direct-detection and indirect-detection experiments⁶⁾.

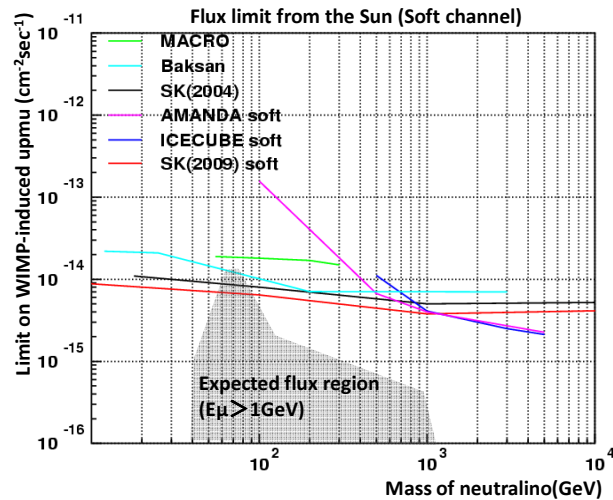


Figure 1: Soft channel flux limits versus WIMP mass.

3. Solar neutrinos

With the combined SK-I, SK-II, SK-III data sets, improved calibrations, a full detector simulation, and improved analysis methods¹⁶⁾, the systematic uncertainty on the observed total solar neutrino flux is reduced to $\pm 2.1\%$, about two thirds the systematic uncertainty for previously published SK-I data¹⁷⁾. The observed 8B solar flux in the 5.0 to 20 MeV total electron energy region is $2.32 \pm 0.04(stat.) \pm 0.05(sys.) \times 10^6 \text{ cm}^{-2} \text{ sec}^{-1}$ under the assumption of pure electron-flavor content, in agreement with previous measurements.

A combined oscillation analysis was carried out using the updated data, by including χ^2 terms corresponding to the SK-I and SK-II spectrum and unbinned time variation, constraining the 8B and *hep* neutrino flux to the SNO NC flux^{18),19)} and Standard Solar Model (SSM) prediction²⁰⁾ respectively. This result (Fig. 4) is consistent with previous SK-I and II results¹⁷⁾, but shows that the energy spectrum and the time variation of the solar neutrino flux as measured by SK now favor only the LMA solution at 95% C.L.

A global two-flavor neutrino oscillation analysis, combining results from other solar neutrino experiments such as SNO, Borexino and radiochemical detectors with the SK-I-II-III combined data, was also performed. For SNO results, the total CC rates observed in the 306-day pure D_2O phase (SNO-I)²¹⁾, 391-day salt phases (SNO-II)²²⁾, and 385-day NCD phase (SNO-III)¹⁸⁾, the combined NC rates of LETA¹⁹⁾ and SNO-III, and the predicted day-night asymmetry for SNO-I and II are used; correlations

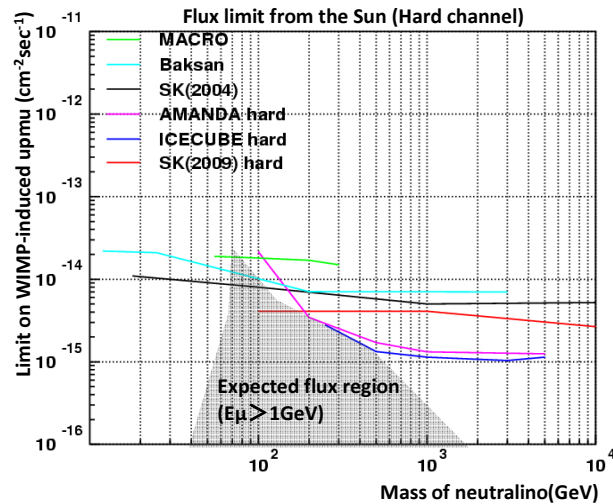


Figure 2: Hard channel flux limits versus WIMP mass.

between the SNO CC and NC rates are not taken into account. Borexino 192-day results ²³⁾, and the Homestake ²⁴⁾, GALLEX-GNO ²⁵⁾, and SAGE ²⁶⁾ data are then added to the global χ^2 , with the flux and their correlations calculated using the SSM as described in ²⁷⁾. The best-fit oscillation parameters are $\sin^2 \theta_{12} = 0.30^{+0.02}_{-0.01}$ ($\tan^2 \theta_{12} = 0.42^{+0.04}_{-0.02}$) and $\Delta m_{21}^2 = 6.2^{+1.1}_{-1.9} \times 10^{-5} eV^2$

Figure 5 shows the 95% allowed region for all solar experiments before and after the SK-III result is included. As shown in the figure, the SK-III result contributes about 5% improvement to the constraints on Δm_{12}^2 .

Combining global solar with KamLAND results, the best-fit parameters become $\sin^2 \theta_{12} = 0.31 \pm 0.01$ ($\tan^2 \theta_{12} = 0.44 \pm 0.03$) and $\Delta m_{21}^2 = 7.6 \pm 0.2 \times 10^{-5} eV^2$.

A three-flavor analysis combining all solar neutrino experiments was also performed, assuming $\Delta m_{23} = 2.4 \times 10^{-3} eV^2$, $\theta_{23} = \pi/4$, and normal hierarchy. The best-fit results are $\sin^2 \theta_{12} = 0.31 \pm 0.03$ ($\tan^2 \theta_{12} = 0.44 \pm 0.06$) and $\Delta m_{21}^2 = 6.0^{+2.2}_{-2.5} \times 10^{-5} eV^2$. Adding KAMLAND data, the results are $\sin^2 \theta_{12} = 0.31^{+0.03}_{-0.02}$ ($\tan^2 \theta_{12} = 0.44^{+0.06}_{-0.04}$) and $\Delta m_{21}^2 = 7.7 \pm 0.3 \times 10^{-5} eV^2$.

Using solar data, the best-fit value for $\sin^2 \theta_{13}$ is 0.01, the upper limit for $\sin^2 \theta_{13}$ is 0.060 at 95% C.L.; adding KamLAND reactor results, the upper limit becomes 0.059 at 95% C.L.. (Figures 6 and 7).

The 8B neutrino flux obtained using oscillation parameters from all solar neutrino experiments is $5.3 \pm 0.2(\text{stat.}+\text{sys.}) \times 10^6 \text{cm}^{-2}\text{sec}^{-1}$; the flux becomes $5.1 \pm 0.1(\text{stat.}+\text{sys.}) \times 10^6 \text{cm}^{-2}\text{sec}^{-1}$ including KamLAND data.

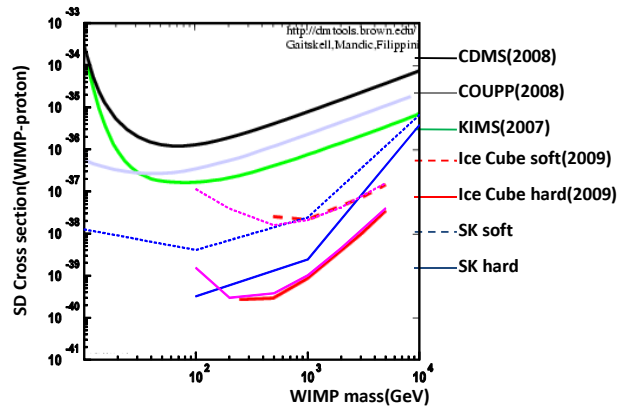


Figure 3: Spin dependent cross sections versus WIMP mass.

4. Supernova Relic Neutrinos

The Supernova Relic Neutrino (SRN) signal has never been seen, although some recent models predict SRN flux close to the discovery thresholds of current experiments^{28) 29)}, motivating further efforts. A new search for SRNs was conducted using SK data covering 2853 days total livetime. Sensitivity is now greatly improved compared to the 2003 SK result³⁰⁾, which had a final model independent flux limit of $1.2\bar{\nu}_e/\text{cm}^{-2}\text{sec}^{-1}$ for neutrino energy > 19.3 MeV, which was ~ 100 times more stringent than the best limit at the time³¹⁾. The new analysis includes a variety of improvements such as increased efficiency, a lower energy threshold, and an expanded data set. New combined upper limits on SRN flux are $2.8 \sim 3.0\bar{\nu}/\text{cm}^{-2}\text{sec}^{-1}$ for total positron energy > 16 MeV.

Results can be compared to models such as the constant SN rate model³²⁾; cosmic gas infall model³³⁾; chemical evolution model³⁴⁾; heavy metal abundance model³⁵⁾; LMA model³⁶⁾; and failed supernova model³⁷⁾. Some examples of theoretical spectra are shown in Fig. 8. Other experiments have also produced SRN limits, such as SNO³⁸⁾ and KamLAND³⁹⁾.

SK can detect SRN events primarily via inverse beta decay ($\bar{\nu}_e + p \rightarrow n + e^+$). The next most visible mode for SRN interactions is about two orders of magnitude less probable. The inverse beta decay cross section used is taken from references^{40) 41)}. SK triggers are based on the number of PMTs detecting light within a 200 ns window (approximately the maximum time for light to traverse the ID). The Low Energy (LE) trigger requires about 29 PMTs (100% efficient at 6.5 MeV, ~ 1 KHz trigger rate), while the Super Low Energy (SLE) triggers (variable threshold between

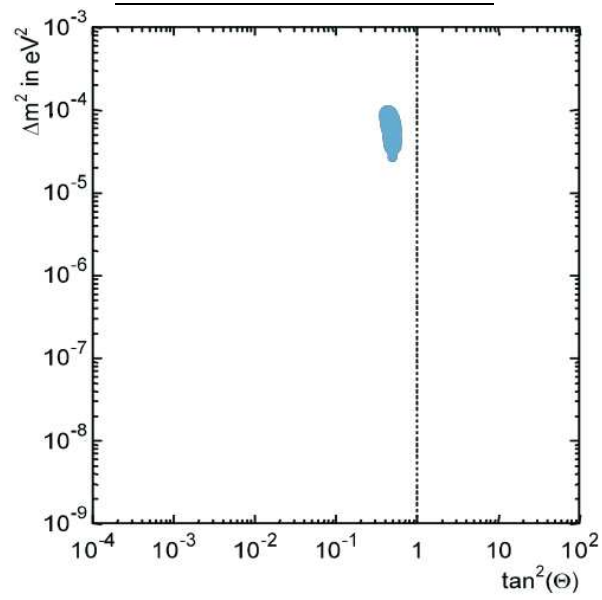


Figure 4: Allowed region (95% CL) from SK-II/II/III data analysis.

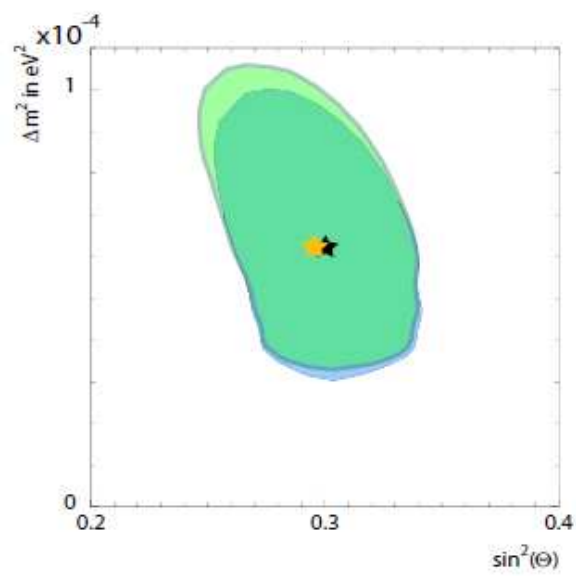


Figure 5: Allowed region for global solar fit for 2-flavor analysis at 95% C.L. Green contour and yellow star show results without SK-III contribution, blue contour and black star show results including SK-III.

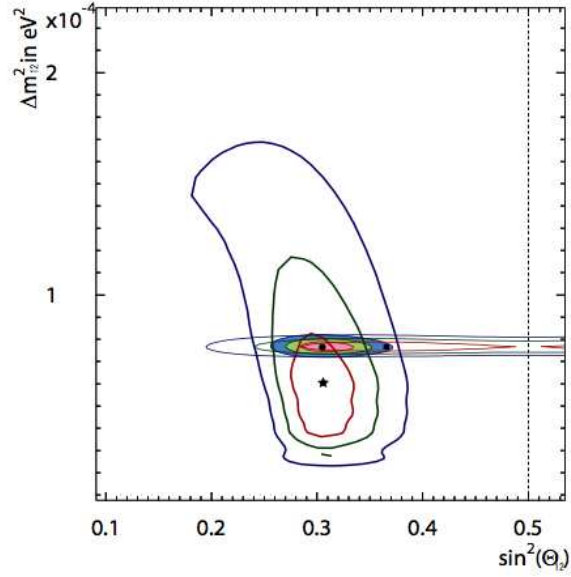


Figure 6: Allowed region in $\Delta m_{12}^2/\theta_{12}$ space from 3-flavor analysis. Thick lines and star are allowed regions (1, 2, 3 σ CLs) from global solar analysis, thin lines are for KAMLAND, and filled areas from combining all solar neutrino experiments and KAMLAND.

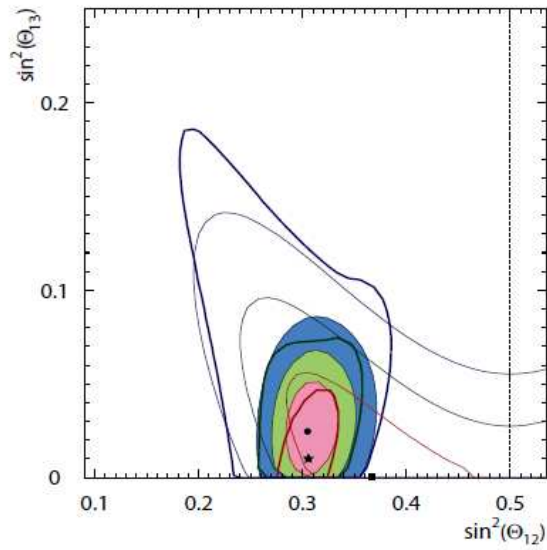


Figure 7: Allowed region in θ_{13}/θ_{12} space from 3-flavor analysis. Same markings as in figure 6.

17 and 24 PMTs, ~ 10 Hz,) has the lowest threshold, requiring dedicated hardware for filtering and reducing the SLE data rate to manageable levels.

With an expected rate of only a few SRN events a year, careful attention to background reduction is necessary. Cuts to remove PMT and electronics noise, and muons are the same as those used for the SK solar neutrino analysis ⁴²⁾. The relic analysis uses the standard SK fully contained, fiducial volume (FC/FV) cuts, rejecting events with OD activity, and requiring event vertices to be more than 2 meters from the ID walls. Cosmic ray muons interacting with an oxygen nucleus cause radioactive spallation, which can mimic the SRN signal. Spallation constitutes the bulk of the SRN background after the noise reduction cut. We correlate relic candidates to previously detected muons, but at low energies, spallation products tend to have long lifetimes. Eventually correlation tagging becomes too inefficient, thus determining the practical lower energy threshold for the analysis.

Four spallation tagging variables are considered: 1) Δt , the amount of time by which the muon preceded the relic candidate trigger; 2) LTRANS, perpendicular distance from the muon track to the relic candidate; 3) QPEAK, the value of the combined charge in the largest nine consecutive bins of the dE/dx histogram; 4) longitudinal distance LLONG, the distance along the muon track from the center of the 9 largest dE/dx bins, where the spallation is expected to occur, to the relic candidate. Probability density functions (PDFs) are formed for each of the four spallation variables and used to define cuts.

After all cuts, four main types of background remain that must be modeled: atmospheric ν_μ and ν_e charged current (CC) events, atmospheric ν neutral current (NC) elastic events, and heavy particle production from atmospheric ν_e . Although other residual backgrounds exist (for example, from multiple and neutral pion production), their contributions were small and their spectral shapes well described by linear combinations of our four modeled backgrounds, and were thus incorporated into the analysis. These backgrounds are modeled using the SK Monte Carlo, based on GEANT 3 and NEUT ¹¹⁾. Hadronic interactions are simulated using a combination of CALOR and custom SK code. For the Michel spectrum (used for the ν_μ CC), we measure the spectrum of decay electrons from cosmic ray muons. The SN relic signal itself is modeled separately, with its own Monte Carlo.

Most of the factors required for a comprehensive prediction of the SRN flux are now fairly well known ⁴⁴⁾, e.g. initial mass functions, cosmic star formation history, Hubble expansion, etc., so we can parameterize typical supernova neutrino emission using two effective parameters ²⁹⁾, ⁴⁵⁾: luminosity from a typical supernova, and average emitted $\bar{\nu}_e$ energy. SRN MC samples were created with a Fermi-Dirac(FD) emission spectrum, at multiple temperatures. For example, the LMA model ³⁶⁾ corresponds to a FD spectrum close to 6 MeV and a $\bar{\nu}_e$ luminosity of 7×10^{45} J. Monte Carlo events were generated from 2.5 to 8 MeV in 0.5 MeV steps, PDFs were parameterized from these spectra, and the final data sample was fitted using these likelihood

functions, assuming $\Omega_m = 0.3$, $\Omega_\Lambda = 0.7$, and $c/H_0 = 4228 \text{Mpc}$. The result is independent of the initial mass function used. Results are shown in Fig. 9 and Fig. 10. Also plotted is the line representing the results of each neutrino temperature analysed separately.

Although our limit is tantalizingly close to the best theoretical predictions, no signal has so far been detected. While SK is expected to continue data taking for many more years, future sensitivity improvements will be slow, since exposure for SK-I/II/III is already 176 kt-years, and the analysis is now highly optimized. 50 kt-years of SK-IV data have already been taken, and the new SK-IV data acquisition electronics may allow for some further background reduction, as decay electrons from atmospheric ν_μ CC interactions can now be tagged by detection of prompt gamma emissions with higher efficiency.

Significant further improvement would be possible by doping SK water with gadolinium, which would lower the energy threshold and backgrounds dramatically, and could allow detection of the SRN signal within five years⁴⁶⁾. Gadolinium-loaded water would permit antineutrino tagging, putting several important low-energy neutrino physics goals within reach for the first time. Tests are now underway using EGADS, a 200-ton prototype system for introducing and removing gadolinium salts from the SK water system. EGADS is nearly complete at time of writing, and will begin tests of long-term stability, materials aging and transparency in late 2011, with results expected in mid-2012⁴⁷⁾.

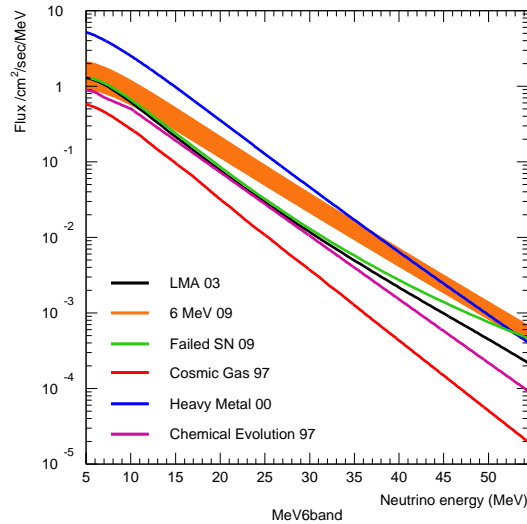


Figure 8: Examples of theoretical model predictions for SRN flux vs energy.

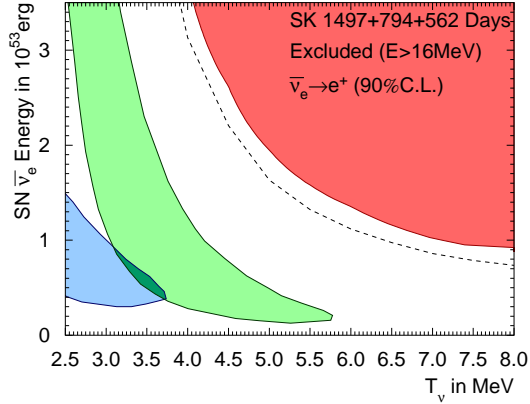


Figure 9: Luminosity vs neutrino temperature excluded region.

5. Test of Apparent CPT Violation Model (ENW Model)

Following publication of results suggesting disagreement between neutrino and antineutrino best-fit Δm^2 values, N. Engelhardt, A.E. Nelson, and J.R. Walsh (ENW) proposed a non-standard interaction model (NSI)⁴⁸⁾ that includes active-sterile neutrino mixing, incorporating a new $U(1)$ gauge force coupled to the difference between baryon and lepton numbers ($B-L$), previously proposed to account for the anomalous results of the MiniBooNE and LSND experiments⁴⁹⁾.

This apparent CPT violation model, referred to here as the ENW Model, uses 3 parameters: m , the active neutrino mass, M , the sterile neutrino mass, and g , the overall matter interaction coupling which includes the Standard Model weak interaction coupling and the coupling from the new $U(1)$ gauge interaction. A non-zero value of M or a value of g larger than the Standard Model's weak interaction Fermi coupling would represent new physics. (See reference⁴⁸⁾ for further details of the model.) These parameters were fitted by ENW with reasonable results to the initial MINOS antineutrino data⁵⁰⁾, although the data used were later updated by MINOS⁵¹⁾.

We have tested the ENW model using all atmospheric neutrino data (fully-, and partially-contained and upward-muon samples) from the SK-I, -II and -III periods. A χ^2 fit was performed, using the same methods and systematic error allowances as in other atmospheric neutrino analyses described here. Central values for the parameters

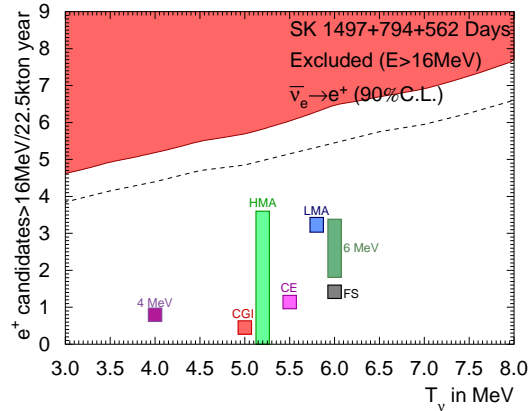


Figure 10: Event rate vs neutrino temperature excluded region.

were as follows: $m = 0.046$ eV, $M = 28.9$ eV, $g = 1.166 \times 10^{-5}$ GeV $^{-2}$, with 99% allowed regions as shown in figure 11. (It should be noted that SK analyses cannot in general place a constraint on the absolute values of neutrino mass, however the ENW model assumes a simplified mass hierarchy where $m_1 = m_2 = 0$). The χ^2 for the fit was 469.1 for 417 degrees of freedom, slightly worse than the standard 2-flavor oscillation best-fit value, which had $\chi^2 = 468.3$ for 418 DOF. Large portions of the ENW parameter space allowed by the early MINOS antineutrino data are ruled out, and the remaining allowed ENW parameter values produce effects almost identical to the SK 2-flavor oscillation results. We conclude that, while not ruled out by the SK data, the ENW model is effectively indistinguishable from ordinary neutrino oscillations using SK data.

6. Acknowledgements

A complete set of acknowledgements for the SK experiment can be found in reference ¹⁶). Personal thanks go to K. Bays, M. Smy, T. Tanaka, R. Wendell, M. Vagins, and especially my student Mike Dziomba, for help preparing the manuscript.

7. References

- 1) Y.Fukuda, *et al.* Phys. Rev. Lett. **81**, 1562 (1998).
- 2) Fukuda, S., *et al.*, Nucl. Instrum. Methods A 501, 418 (2003).

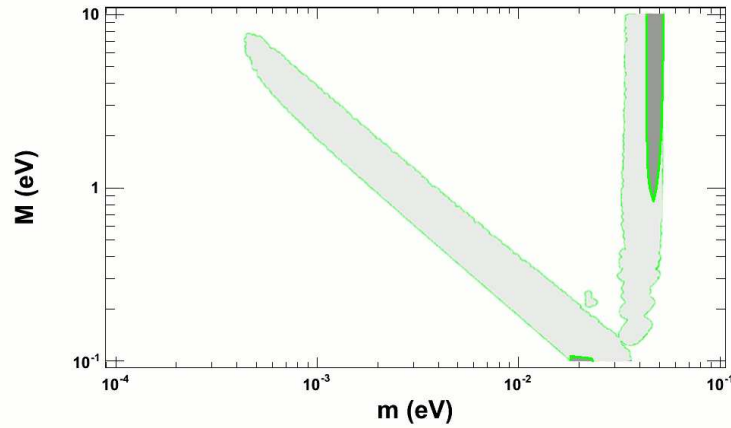


Figure 11: Allowed regions for ENW model parameters M and m , showing 99% CL allowed regions from SK data.

- 3) Ashie, Y., *et al.* Phys. Rev. D71, 112005 (2005), hep-ex/0501064.
- 4) M. Drees and M. M. Nojiri, Phys. Rev. D 47, 376 (1993)
- 5) C. Amsler *et al.*, Phys. Lett. B 667, 1 (2008)
- 6) R. C. Gilmore, Phys. Rev. D 76, 043520 (2007)
- 7) S. Desai *et al.*, Super-K collaboration, Phys. Rev. 70, 083523 (2004)
- 8) M. Blennow, J. Edsjö, T. Ohlsson, JCAP 0801, 021 (2008)
- 9) P. Gondolo, J. Edsjö, P. Ullio, L. Bergst, M. Schelke and E. A. Baltz, JCAP 0407, 008 (2004)
- 10) T. Tanaka, *et al.*, Super-Kamiokande Collaboration, arXiv:1108.3384, accepted by Astrophys. J. (2011).
- 11) Y. Hayato, Nuclear Physics B (Proc. Suppl.) 112 (2002)
- 12) M. Honda *et al.*, Phys. Rev. D 75, 043006 (2007)
- 13) L. V. Volkova, Sov. J. Nucl. Phys. 31, 784 (1980)
- 14) Y. Ashie *et al.*, Super-Kamiokande Collaboration, Phys. Rev. Lett. 93, 101801 (2004)
- 15) G. Wikström and J. Edsjö, JCAP 04, 009 (2009)
- 16) The Super-Kamiokande Collaboration, Phys. Rev. D 83, 052010 (2011), arXiv:1010.0118.
- 17) The Super-Kamiokande Collaboration, Phys. Rev. D 73, 112001 (2006), hep-ex/0508053.
- 18) B. Aharmim *et al.*, Phys. Rev. Lett. 101 111301 (2008).
- 19) B. Aharmim *et al.*, Phys. Rev. C 81 055504 (2010).
- 20) J.N. Bahcall and M.H. Pinsonneault, Phys. Rev. Lett. 92 121301 (2004).
- 21) B. Aharmim *et al.*, Phys. Rev. C, 75 045502 (2007).

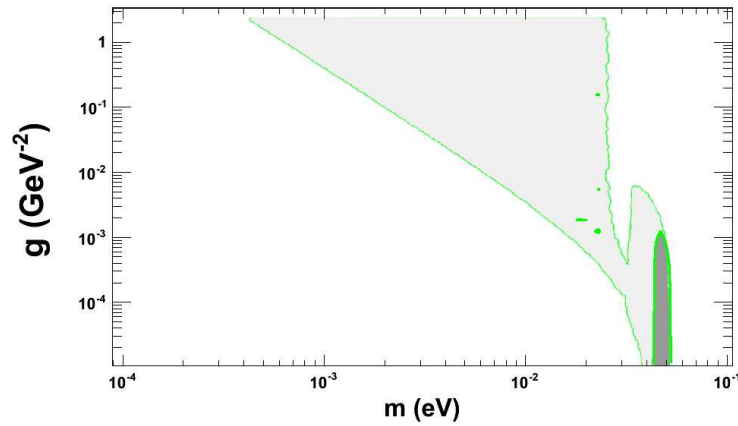


Figure 12: Allowed regions for ENW model parameters g and m , showing 99% CL allowed regions from SK data.

- 22) S.N.Ahmed *et al.*, Phys. Rev. C. 72 055502 (2005).
- 23) C.Arpesella *et al.*, Phys. Rev. Lett. 101 091302 (2008).
- 24) B.T.Cleveland *et al.*, Astrophys. J. 496 505 (1998).
- 25) M.Altmann *et al.*, Phys. Lett. B490 16 (2000).
- 26) J.N.Abdurashitov *et al.*, Phys. Rev. C60 055801 (1999).
- 27) G.L.Fogli *et al.*, Phys. Rev. D66 05310 (2002).
- 28) L. Strigari, M. Kaplinghat, G. Steigman, and T. Walker, Journal of Cosmology and Astroparticle Physics 0403:007 (2004).
- 29) S. Horiuchi, J. F. Beacom, and E. Dwek, Phys. Rev. D 79, 083013 (2009).
- 30) M. Malek *et al.* (The Super-Kamiokande Collaboration), Phys. Rev. Lett. 90, 061101 (2003), arXiv:hep-ex/0209028.
- 31) W. Zhang *et al.* (The Kamiokande Collaboration), Phys. Rev. Lett. 61, 385 (1988).
- 32) T. Totani, K. Sato, and Y. Yoshii, Astrophysical Journal 460, 303 (1996), arXiv:astro-ph/9509130.
- 33) R. A. Malaney, Astroparticle Physics 7, 125 (1997).
- 34) D. H. Hartmann and S. E. Woosley, Astroparticle Physics 7, 137 (1997).
- 35) M. Kaplinghat, G. Steigman, and T. P. Walker, Phys. Rev. D 62, 043001 (2000).
- 36) S. Ando, K. Sato, and T. Totani, Astroparticle Physics 18, 307 (2003). The flux of the LMA model is increased by a factor of 2.56 from the paper, a revision introduced at NNN05.
- 37) C. Lunardini, Phys. Rev. Lett. 102, 231101 (2009).
- 38) B. Aharmim *et al.* (SNO), Astrophys. J. 653, 1545 (2006), arXiv:hep-

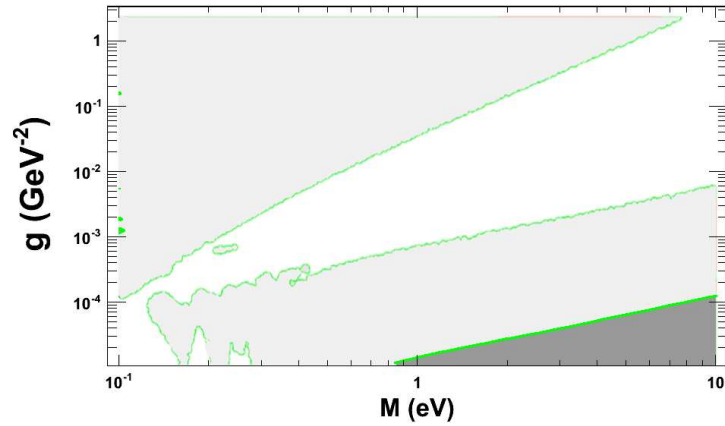


Figure 13: Allowed regions for ENW model parameters g and M , showing 99% CL allowed regions from SK data.

ex/0607010.

- 39) The KamLAND Collaboration, (2011), arXiv:1105.3516 [astro-ph.HE].
- 40) A. Strumia and F. Vissani, Phys. Lett. B564, 42 (2003), arXiv:astro-ph/0302055.
- 41) P. Vogel and J. F. Beacom, Phys. Rev. D 60, 053003 (1999).
- 42) J. Hosaka *et al.* (The Super-Kamiokande Collaboration), Phys. Rev. D 73, 112001 (2006).
- 43) J. P. Cravens *et al.* (The Super-Kamiokande Collaboration), Phys. Rev. D 78, 032002 (2008).
- 44) J. F. Beacom, Ann. Rev. Nucl. Part. Sci. 60, 439 (2010), arXiv:1004.3311 [astro-ph.HE].
- 45) H. Yüksel, S. Ando, and J. F. Beacom, Phys. Rev. C 74, 015803 (2006).
- 46) J. F. Beacom and M. R. Vagins, Phys. Rev. Lett. 93, 171101 (2004).
- 47) M. Vagins, private communication.
- 48) N. Engelhardt, A. E. Nelson, and J. R. Walsh, “Apparent CPT Violation in Neutrino Oscillation Experiments”, arXiv:1002.4452 [hep], 2010.
- 49) A. E. Nelson and J. Walsh, Phys. Rev. D77, 033001 (2008), 0711.1363.
- 50) MINOS Collaboration, Phys.Rev.D81:072002,2010.
- 51) MINOS Collaboration, arXiv:1007.2791 [hep-ex].